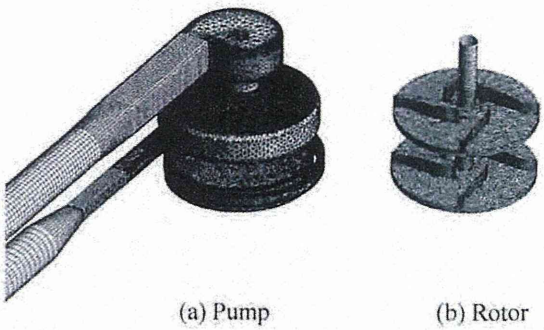

(a) Pump (b) Rotor

Fig. 4 Computational grid on the pump and the rotor

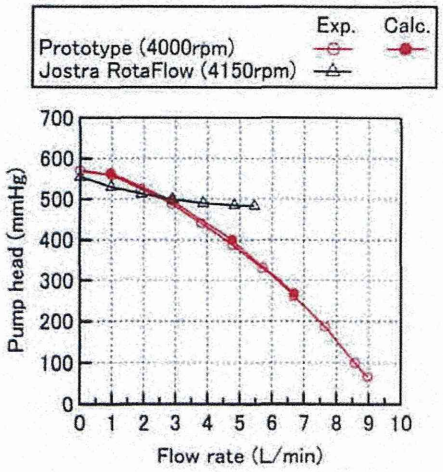

Fig. 5 Pump performance

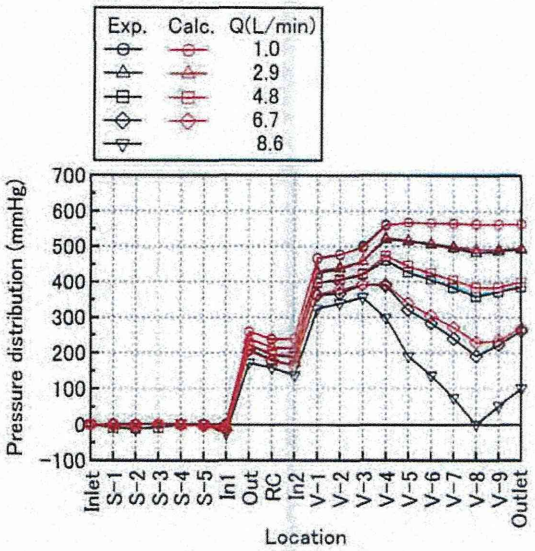

Fig. 6 Pressure distribution in the pump

5. Results and Discussions

5.1 Performance Curve

Figure 5 shows a performance curve of the prototype. The horizontal and vertical axes mean the flow rate and the pump head, respectively. The experiment was conducted with the rotational speed of 1200 rpm using the water and the results were converted into the values in the operation with the blood at 4000 rpm, considering an easy understanding in clinical practice. The demanded pump performance of 500 mmHg at 3 L/min was obtained at 4000 rpm in the experiment with the blood, although the design rotational speed was 4200 rpm. Therefore, the results were converted into the values at 4000 rpm, using the relation of $\Delta p_{blood} = \Delta p_{water} \cdot \rho_{blood} \cdot U_{t,blood}^2 / (\rho_{water} \cdot U_{t,water}^2)$ derived from the condition that the values of the pressure coefficients in the operations with the water and the blood are the same because the Reynolds numbers are equal and the flow fields are hydrodynamically similar in both cases.

As a reference pump, the Jostra RotaFlow centrifugal pump (Maquet Cardiopulmonary AG) was used, which is of practical use and is considered to have high anti-hemolysis performance. The pump performance of the Jostra RotaFlow centrifugal pump is also shown in Fig.5. The results was obtained through translating the results of 1200 rpm with the water into the results of 4150 rpm with the blood. The slope of the performance curve of the prototype is steeper than that of the Jostra RotaFlow centrifugal pump in usable ranges of 1 - 5 L/min. This means that the prototype has useful characteristics that the flow rate is insensitive to the flow resistance. The results of the CFD for the prototype is also shown in Fig.5 and agree with experimental results well.

The efficiency of the prototype was also measured. As the torque generated by the friction between the shaft and the seal was different case by case in the operation using the air as a working fluid, there was variation in the efficiency obtained by substituting the torque with the air from that with the water. In the operation using the water, the torque generated by the friction between the shaft and the seal was stable. The efficiency including the friction between the shaft and the seal was 5 - 8 % at $Q=Q_d$ (3 L/min) and the maximum efficiency was 6 - 10 % at 5 L/min.

5.2 Pressure Distribution

The pressure distribution in the pump was measured at 0.29, 0.86, 1.43, 2.00, 2.57 L/min at 1200 rpm and shown in Fig.6. These

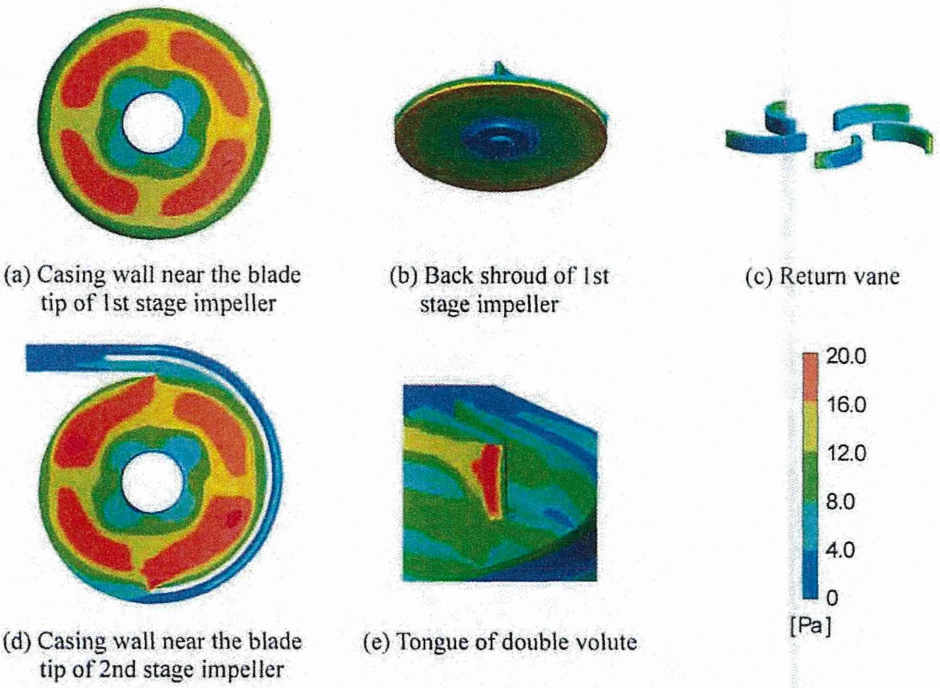

(a) Casing wall near the blade tip of 1st stage impeller

(b) Back shroud of 1st stage impeller

(c) Return vane

(d) Casing wall near the blade tip of 2nd stage impeller

(e) Tongue of double volute

Fig. 7 Wall shear stress distribution in the pump at $Q=Q_d$. N=1150 rpm

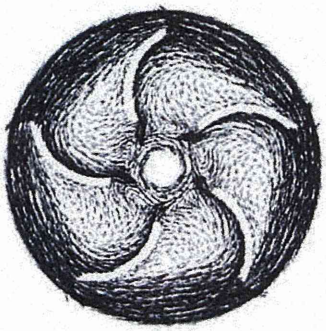

Fig. 8 Velocity vector on the cross-section (D'-D' in Fig.1) of the return channel at $Q=Q_d$. N=1150 rpm. The distance of the cross-section D'-D' from the casing wall is 0.5 mm.

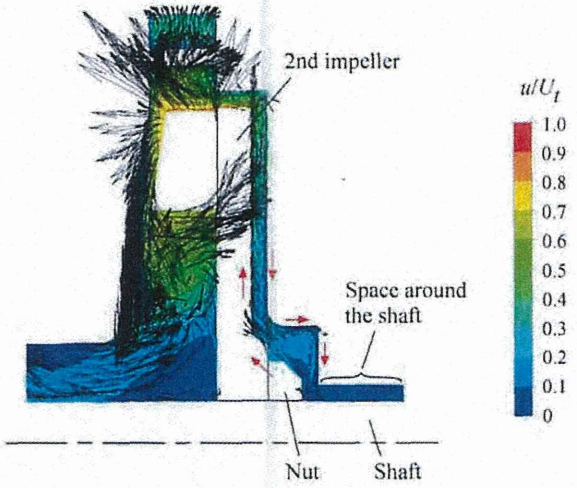

Fig. 9 Flow field on the meridian plane around the rear space of the back shroud of the 2nd stage impeller at $Q=Q_d$. N=1150 rpm.

flow rates corresponds to 1.0, 2.9, 4.8, 6.7, 8.6 L/min at the operation of 4000 rpm using the blood as a working fluid. The horizontal axis means positions shown in Fig.2. The values of In 1, Out, RC, In 2 are the averaged values of circumferential pressure distribution. The computational results are in good agreement with the experimental results except for the positions from V-5 to V-9 at higher flow rates (4.8 L/min and 6.7 L/min).

The pump head generated by the 1st and 2nd stage impellers are nearly same due the pre-swirl flow in the suction volute and the incomplete turning in the return guide vane. The pressure recovers smoothly in the double volute (V-1 to V-4) except for the case with the higher flow rate of 8.6 L/min.

5.3 Anti-Hemolysis Performance

Kameneva et al. [9] examined the blood flow in a narrow tube with the inner diameter of 1 mm and showed that the amount of the hemolysis drastically increased when the shear stress on the blood was larger than 200 Pa. Therefore, the shear stress of 200 Pa

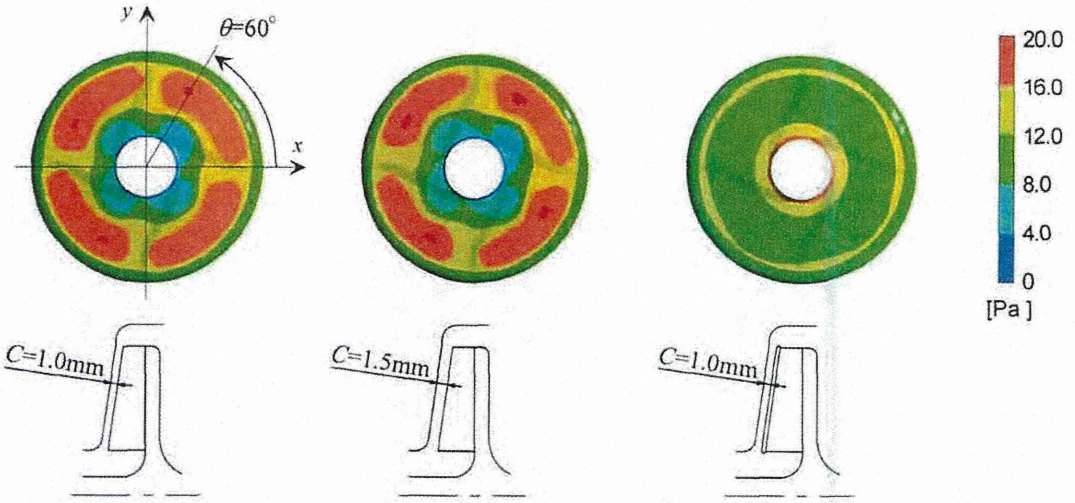

(a) C=1 mm (b) C=1.5 mm (c) C=1 mm with front shroud

Fig. 10 The effects of tip clearance and front shroud for wall shear stress on the casing wall near the 1st stage impeller. N=1150 rpm

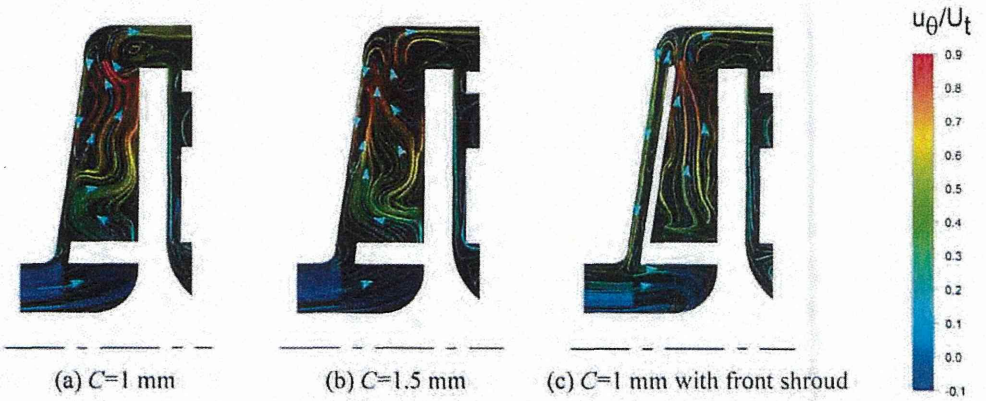

(a) C=1 mm (b) C=1.5 mm (c) C=1 mm with front shroud

Fig. 11 Streamline on meridian plane around the 1st stage impeller at θ=60 deg, defined in Fig.10(a)

was used as a threshold of hemolysis in the present study. The wall shear stress in the pump is shown in Fig.7. In the operation of 1150 rpm with the water, the threshold of the shear stress for the hemolysis is about 16 Pa, based on the similarity law of $\tau_{water} = \tau_{blood} \cdot \rho_{water} \cdot U_{t,water}^2 / (\rho_{blood} \cdot U_{t,blood}^2)$. The shear stress larger than 16 Pa is observed on the casing wall near the tip of the 1st and 2nd impellers (Fig.7(a) and (d)), the periphery of the backshroud of the 1st impeller (Fig.7(b)), and the tongue of the double volute casing (Fig.7(e)). The reduction of these high shear stress is necessary to suppress the hemolysis.

5.4 Anti-Thrombosis Performance

Figure 8 shows the velocity vector on the cross-section D'-D' in Fig.1, which is in the return channel and near the casing wall (0.5 mm from the wall). As shown in Fig.8, the flow separates from the blade and the stagnation occurs in the center of the vortex, which can cause the thrombosis.

Figure 9 shows the flow field in the meridian cross-section around the clearance between the backshroud of the 2nd impeller and the casing. The fluid in the boundary layer of the backshroud flows outward, driven by the centrifugal force due to the rotation of the impeller. The outward flow generates the inward flow near the casing, the recirculating flow occurs in the clearance. However, as the velocity is small near the shaft, it was suggested that the 2nd impeller should have a washout hole to suppress the thrombosis. The velocity in the space around the shaft is also small and should be removed for the suppression of the thrombosis. The spaces with the possibility of the thrombosis will be removed in next prototype.

5.5 Reduction of the High Wall Shear Stress on the Casing Wall near the Blade Tip of the Impeller

It is considered that an optimal tip clearance exists for the suppression of the hemolysis. In the study of Schima et al. [4], the amount of the hemolysis became smallest in the case with the tip clearance of 1.5 mm in a single stage centrifugal pump. Therefore, we conducted the computation for the pump with the tip clearance of 1.5 mm. Figure 10 shows the wall shear stress on the casing

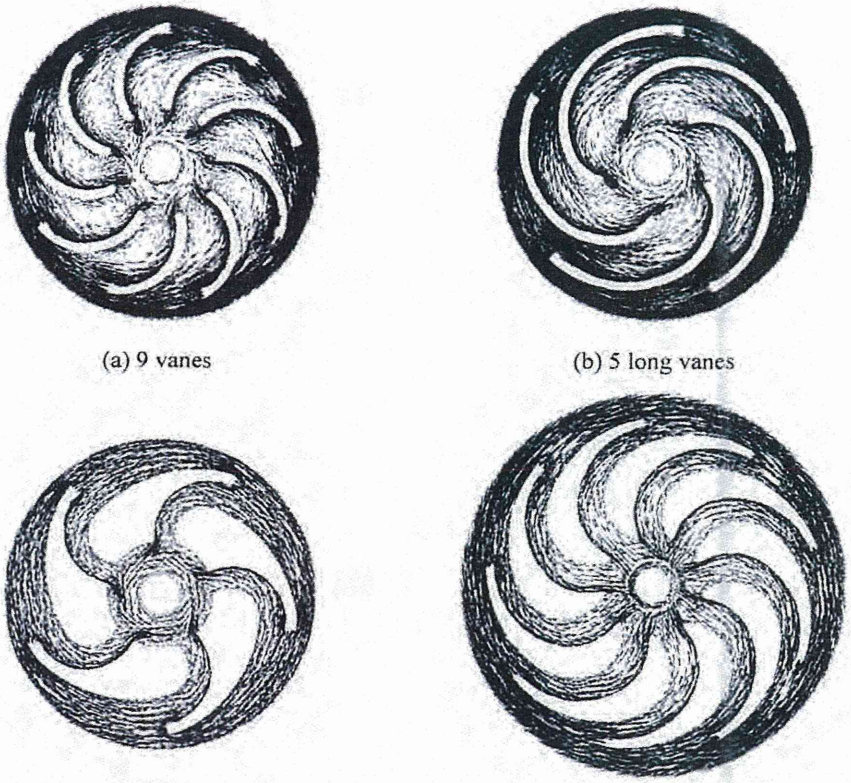

(a) 9 vanes (b) 5 long vanes

(c) 5 thicker vanes (d) 9 thicker vanes

Fig. 12 Velocity vector near the casing in various types of return guide vane (return channel)

near the blade tip of the 1st impeller. Figures 10 (a) and (b) show the results for C=1 mm and 1.5 mm, respectively. The results shown in Figs.7(a) and 10(a) are a little different due to the difference of the return channel. It could be confirmed that the region with the shear stress higher than 16 Pa decreases due to the increase of the tip clearance, but the amount of the reduction of high shear stress region was small. Figure 10(c) shows the results in the case of the impeller with a front shroud and the clearance of C = 1 mm. The front shroud was quite effective for reducing the high shear stress region.

Figure 11 shows streamlines around the 1st impeller on the meridian cross-section at θ=60 deg shown in Fig.10(a). The color of the streamlines means the ratio of the circumferential velocity u_θ to the tip speed U_t. Figures 11(a), (b), (c) show the results of C = 1 mm, 1.5 mm, and 1 mm with the front shroud, respectively. As shown in Figs.11(a) and (b), a larger circumferential velocity occurred near the casing wall around the tip of the impeller. This is the cause of the higher wall shear stress on the casing near the tip of the impeller. In the case with the front shroud, the occurrence of the higher velocity near the casing is suppressed as shown in Fig.11(c) and this leads to the suppression of the higher shear stress.

The pump head in the cases with C=1 mm, 1.5 mm, and 1 mm with the front shroud are 485 mmHg, 463 mmHg, and 538 mmHg, respectively, and the pump head increased by about 11% using the front shroud. Kurokawa et al. [10] reported that the head of the pump with a low specific speed increases using the front shroud. As the increase of the pump head results in a low rotational speed of the impeller, the front shroud has an advantage for the anti-hemolysis performance.

5.6 Modification of the Return Guide Vane

As shown in Fig.8, in the return channel, the stagnation which could be the cause of the thrombosis occurred at the center of the steady vortex due to the flow separation. Therefore, the geometry of the return guide vane (return channel) was considered to suppress the stagnation. The geometries of various types of the return guide vane (return channel) we considered and the velocity field were shown in Fig.12. The vane angles of pressure surface at the inlet and the outlet are 2 deg and 90 deg, respectively. To increase the effect of the return guide vane, the number of the vanes was increased from 5 to 9 and the flow field in the case with 9 guide vanes was shown in Fig.12(a). Although the size of the vortex diminished in comparison with Fig.8, the stagnation at the center of vortex due to the flow separation occurred.

The height of the return guide vane in the present study was larger so as to be equal to the larger blade height of the impeller. For this reason, the circumferential velocity is quite larger than the radial velocity in the return channel. Therefore, longer guide vane was tried to be adopted to turn the flow gradually from the circumferential direction to the radial direction. The flow field for the longer guide vane is shown in Fig.12(b). Larger flow separation was suppressed by the longer guide vane, but the flow was not along the guide vane near the outlet of the return channel and the circumferential velocity could not be decreased well. In the above modifications, the vane with a constant thickness was adopted for easy designing of the vane but was difficult to suppress the flow separation. Then, we gave the thickness to the guide vane such that the vane covers the region of the flow separation shown in Fig.8.

The flow field for the thicker guide vane is shown in Fig.12(c) and we find the flow stagnation disappears. The design method of the return guide vane which covers the region of the flow separation is effective for the suppression of the stagnation, although the method is a trial-and-error method. In the case with the small number of the vanes such as 5, the vane is quite thick and the flow stagnation can occur near the trailing edge of the vane. Then, we designed the guide vane which covered the region of the flow separation shown in Fig.12(a) for 9 vanes. The flow field for 9 thick guide vanes is shown in Fig.12(d). Although the result is for another pump similar to the present pump, the flow separation is suppressed and the circumferential velocity is decreased well. It was found that the design method of the return guide vane which covers the region of the flow separation is effective for the suppression of the stagnation. We also found that the increase of the number of the vanes leads to the decrease of the region of the flow separation and the vane thickness and is effective for decreasing the circumferential velocity well at the outlet of the return channel.

The amplitude of the pressure fluctuation at the outlet was from -13% to +10% of the average values in the original pump and was from -7% to +4% in the pump with five thicker vanes. In both cases, the pressure fluctuations were mainly caused by the interaction of the wake of the impeller and the tongue of the double volute casing because of the smaller clearance of 2 mm between the outlet of the impeller and the tongue of the double volute casing, although the geometry of the return guide vanes affect the pressure fluctuation at the outlet to a certain degree. As the pump with 9 thicker vanes has the larger clearance of 7 mm between the outlet of the impeller and the tongue of the double volute casing, the amplitude of the pressure fluctuation at the outlet was smaller and about ±1% of the average values. Therefore, as you know, the larger clearance between the outlet of the impeller and the tongue of the volute casing is effective for the suppression of the pressure fluctuation. The larger distance is also effective for the decrease of the shear stress on the tongue, which is reported in detail in the next paper.

6. Conclusions

We carried out the research on the development of a two-stage centrifugal blood pump for the cardiopulmonary support system. The two-stage blood pump in the present study is characterized by higher discharge pressure at low peripheral speed of the impeller. The results obtained in the present study are summarized as follows.

(1) The slope of the performance curve of the prototype is larger. This means that the prototype has useful characteristics that the flow rate is insensitive to the resistance.
(2) The higher shear stress which can cause the hemolysis occurs on the casing near the tip of the impeller and the flow stagnation which can be a cause of the thrombosis occurs in the return channel if we design a centrifugal blood pump with a low type number and a semi-open impeller, mainly based on the design method for general industrial pumps.
(3) The enlargement of the tip clearance was not effective for decreasing the wall shear stress on the casing near the tip of the impeller.
(4) The front shroud of the impeller suppresses the interaction between the secondary flow and the casing and can decrease the wall shear stress on the casing near the tip of the impeller. As the front shroud increases the pump head, it can be useful to increase the anti-hemolysis performance by decreasing the rotational speed of the impeller.
(5) It was found that the design method of the return guide vane which covers the region of the flow separation is effective for the suppression of the stagnation. We also found that the increase of the number of the vanes leads to the decrease of the region of the flow separation and the vane thickness and is effective for decreasing the circumferential velocity well at the outlet of the return channel.

Improvements of the present pump and the result of the hemolysis test are reported in a next paper.

Acknowledgments

The present study was supported by JSPS Grant-in-Aid for Scientific Research (B) (Grant Number 18360094, Principal Investigator: Dr. Tomonori Tsukiya).

Nomenclature

C	Tip clearance	ν	Kinetic viscosity
D_t	Diameter of impeller	θ	Circumferential coordinate
h	Blade height	ρ	Fluid density
N	Rotational speed	τ	Shear stress
Q	Volumetric flow rate	**Subscript**	
Re	Reynolds number ($=U_tD_t/\nu$)	1	Inlet
u	Flow velocity	2	Outlet
U_t	Tip speed of impeller	*blood*	Blood
β	Blade angle	d	Reference
Δp	Pressure difference	*water*	Water
μ	Viscosity	θ	Circumferential component

References

[1] Horiguchi, H., Tsukiya, T., Takemika, T., Nomoto, T., and Tsujimoto, Y., 2013, "Improvement of Two-Stage Centrifugal Blood Pump for Cardiopulmonary Support System and Evaluation of Anti-Hemolysis Performance (in Japanese)," Transactions of the

JSME, Series B, Vol. 79, No. 800, pp. 11-23.
[2] Lou, S., MacLaren, G., Best D., Delzoppo, C., and Butt, W., 2014, "Hemolysis in Pediatric Patients Receiving Centrifugal-Pump Extracorporeal Membrane Oxygenation: Prevalence, Risk Factors, and Outcomes," Critical Care Medicine, Vol. 42, No. 5, pp. 1213-1220.
[3] Takeda, H., 2005, "Basic Design on Pumps (in Japanese)," Dengyosha Technical Review, Vol. 29, No. 2, pp. 7-14. (http://www.dmw.co.jp/technical/pdf/no57.pdf)
[4] Schima, H., Muller, M. R., Papantonis, D., Schlusche, C., Huber, L., Schmidt, C., Trubel, W., Thoma, H., Losert, U., and Wolner, E., 1993, "Minimization of Hemolysis in Centrifugal Blood Pumps: Influence of Different Geometries," The International Journal of Artificial Organs, Vol. 16, No. 7, pp. 521-529.
[5] Miyazoe, Y., Sawairi, T., Ito, K., Konishi, Y., Yamane, T., Nishida, M, Masuzawa, T., Takiura, K., and Taenaka, Y., 1998, "Computational Fluid Dynamic Analysis to Establish Design Process of Centrifugal Blood Pumps," Artificial Organs, Vol. 22, No. 5, pp. 381-385.
[6] Masuzawa, T., Tsukiya, T., Endo, S., Tatsumi, E., Taenaka, Y., Yamane, T., Nishida, M., Asztalos, B., Miyazoe, Y., Ito, K., Sawairi, T., and Konishi, Y., 1998, "Effect of Gaps Between Impeller Tip and Casing Wall upon Hemolysis Property of a Centrifugal Blood Pump (in Japanese)," Journal of Life Support Engineering, Vol. 10, No. 3, pp. 102-105. (https://www.jstage.jst.go.jp/article/lifesupport1996/10/3/10_3_102/_pdf)
[7] ANSYS, Inc., 2006, "Modeling Flow Near the Wall", ANSYS CFX-Solver Modeling Guide, Release 11, pp.125-127.
[8] ANSYS, Inc., 2006, "Modeling Flow Near the Wall", ANSYS CFX-Solver Theory Guide, Release 11, pp.110-111.
[9] Kameneva, M. V., Burgreen, G. W., Kono, K., Repko, B., Antaki, J. F., and Umezu, M., 2004, "Effects of Turbulent Stresses upon Mechanical Hemolysis: Experimental and Computational Analysis," ASAIO Journal, Vol. 50, No. 5, pp. 418-423.
[10] Kurokawa, J., Choi, Y-D., Ishii, M., Matsui, J., and Imamura, H., 2003, "Theoretical Head of Semi-Open Impeller," Proceedings of the 7th Asian International Conference on Fluid Machinery, No. 40030, pp. 1-7.

J Artif Organs
DOI 10.1007/s10047-014-0811-z

ORIGINAL ARTICLE

Artificial Heart (Basic)

Development of a flow rate monitoring method for the wearable ventricular assist device driver

Kentaro Ohnuma · Akihiko Homma · Hirohito Sumikura · Tomonori Tsukiya · Yoshiaki Takewa · Toshihide Mizuno · Hiroshi Mukaibayashi · Koichi Kojima · Kazuo Katano · Yoshiyuki Taenaka · Eisuke Tatsumi

Received: 9 July 2014 / Accepted: 5 December 2014

Abstract Our research institute has been working on the development of a compact wearable drive unit for an extracorporeal ventricular assist device (VAD) with a pneumatically driven pump. A method for checking the pump blood flow on the side of the drive unit without modifying the existing blood pump and impairing the portability of it will be useful. In this study, to calculate the pump flow rate indirectly from measuring the flow rate of the driving air of the VAD air chamber, we conducted experiments using a mock circuit to investigate the correlation between the air flow rate and the pump flow rate as well as its accuracy and error factors. The pump flow rate was measured using an ultrasonic flow meter at the inflow and outflow tube, and the air flow was measured using a thermal mass flow meter at the driveline. Similarity in the instantaneous waveform was confirmed between the air flow rate in the driveline and the pump flow rate. Some limitations of this technique were indicated by consideration of the error factors. A significant correlation was found between the average pump flow rate in the ejecting direction and the average air flow rate in the ejecting direction ($R^2 = 0.704$–0.856), and the air flow rate in the filling direction ($R^2 = 0.947$–0.971). It was demonstrated that the average pump flow rate was estimated exactly in a wide range of drive conditions using the air flow of the filling phase.

Keywords Flow rate monitoring · Wearable pneumatic drive unit · Ventricular assist devices (VADs) · Air mass flow

K. Ohnuma (✉) · H. Sumikura · T. Tsukiya · Y. Takewa · T. Mizuno · Y. Taenaka · E. Tatsumi
Department of Artificial Organs, National Cerebral and Cardiovascular Center Research Institute, 5-7-1 Fujishirodai, Suita-shi, Osaka 565-8565, Japan
e-mail: ohnuma.kentaro@ri.ncvc.go.jp

A. Homma · K. Katano
School of Science and Engineering, Tokyo Denki University, Saitama, Japan

H. Mukaibayashi · K. Kojima
IWAKI Co., Ltd., Saitama, Japan

Published online: 13 December 2014

Introduction

Mechanical circulatory support using ventricular assist devices (VADs) has become a major option in the treatment of severe heart failure. Early VADs were used mainly as a bridge to heart transplantation (BTT). For BTT patients to be discharged and stay at home, the blood pump needs to be implanted; therefore, a wide variety of implantable devices have been developed [1, 2]. Annually, more than 1,000 patients are implanted with the current devices that use compact rotary pumps [2–4]. An overwhelming shortage of donor organs, however, is still a serious problem globally. Organ transplantation from brain-death donors was approved in 1997 in Japan [5], but the accumulative number of heart transplantations as of December 2013 was only 186.

Before two types of implantable VADs were approved in Japan in 2010 [6], the extracorporeal VAD with a pneumatically driven pump, originally developed at the National Cerebral and Cardiovascular Center, was the only VAD available in Japan (currently available as Nipro VAD, Nipro, Osaka, Japan) [7–11]. More than 900 patients have been treated with Nipro VAD, and about 50 patients are almost always being treated with this system in Japan [12]. The Nipro VAD has played an important role as a chronic-use device for patients, who are outside the

application range of transplantation or not suitable for implantable VAD due to small body size, or as a temporary support for a bridge to decision [2, 6] in the acute severe heart failure patients.

The conventional driver of this pneumatic VAD is equipped with an air compressor, vacuum pump, and batteries. These components, however, make the driver heavy and bulky, which restricts the activity of the patients. Downsizing of the pneumatic VAD driver is one of the key factors for improving the patient's QOL by expanding the range of actions. The authors developed a portable driver for the Nipro VAD, the Mobart-NCVC driver (Senko Medical Instrument Manufacturing Co., Ltd.), which allows transportation in the hospital by the patient himself, and also enables long-distance transportation of patients from one institute to another for heart transplantation. The Mobart-NCVC uses an electro-hydraulic actuator and weighs 13 kg [13].

Our research institute has been working on the development of a more compact VAD driver consisting of a cylinder-piston actuator [14]. The current model of this driver, including its two batteries, weighs only 4.7 kg. The pump can be operated with the two batteries for more than 5 h under normal operating conditions. We are planning to add an additional flow meter to this driver, which will be useful to optimize the operating conditions of the VAD. A mass flow meter, which is capable of measuring the instantaneous flow rates of the driving air in the VAD air chamber, has been employed to calculate blood flow through the VAD. The present study introduces the air flow meter for our portable VAD driver and examines accuracy and errors of it in relation to the pump flow through experiments using a mock circuit. Correction methods for obtaining blood flow rates from the air flow rates are also investigated.

Materials and methods

Description of Nipro VAD blood pump

The Nipro VAD blood pump is a pneumatically driven diaphragm pump, as shown in Fig. 1b. The blood pump is mainly made from polyurethane resin (TM3) and consists of two mechanical heart valves. The priming volume of the blood pump is 70 mL, and is capable of generating 50–60 mL of blood flow per beat.

Wearable pneumatic drive unit (WPD)

The structure of the mechanism in the WPD for generating air pressure is depicted in Fig. 1. Air pressure to drive the diaphragm of the blood pump is generated by converting the rotation of the brushless DC motor into linear motion via a crankshaft directly connected to the cylinder piston. The internal capacity of this cylinder piston is 109 mL. Two regulating valves at the air outlets adjust the driving positive or negative pressure by releasing or drawing the air from or into the tube. The ratio of systole duration (SD) is predetermined by the built-in noncircular gears [14]. The current model of the WPD is also equipped with a pressure release valve at the bottom dead center to compensate for any change in the amount of air in the air circuit due to air leaks from pressure control or changes in room air conditions. The top dead center and bottom dead center of the cylinder piston can be detected with built-in proximity sensors. The experiments in the present study were conducted using three drive units with SD ratios of 35, 40, and 45 % (WPD100-SD35, SD40, and SD45).

Measurement of air flow rates

Figure 2 shows the experimental setup. The Nipro VAD blood pump was connected to an overflow-type mock circuit (IWAKI Co., Ltd.). The working fluid was tap water at 25 °C. The WPD was connected to the Nipro VAD via a 1.35-m air driveline. The air flow rates in the driveline were measured using a thermal gas mass flow meter (model 4043, TSI Inc.), which was installed in the driveline 750 mm away from the blood pump. This mass flow meter possesses a good accuracy (up to 2 % or 0.05 L/min) and response (4 ms) with low resistance. The measurement of the reverse flow with this flow meter has the uncertainty of 2.5 % of the reading in comparison with it of the flow of the forward direction. The forward direction of the flow meter was set as the ejecting direction of VAD. The flow rates of the blood pump were measured using ultrasonic flow meters (T106, Transonic Systems Inc.) installed in the tubes on the inflow and outflow sides of the pump. The air pressures of the WPD were measured using piezoelastic pressure transducers (PA-500, Nidec Copal Electronics Corp.). The position of the cylinder piston was detected from the pulse signals at the top dead center and bottom dead center of the cylinder piston. The flow meter was able to output the volumetric flow rates under a standard condition (at 21.11 °C and 101.3 kPa). Because the pressure in the driveline widely varied during pump operation, flow rates were corrected using the following equation:

$$Q_{aVF} = Q_{aStdF}\left[\frac{273.15+T}{273.15+21.11}\right]\left[\frac{759.8}{759.8+P}\right] \quad (1)$$

where $Q_{a\ VF}$ is the converted volumetric flow rate of the air driveline, $Q_{a\ StdF}$ is the reading from the flow meter, P is the pressure of the driveline, and T is temperature of the air (°C). T was approximately assumed room temperature because it was difficult to exactly measure the

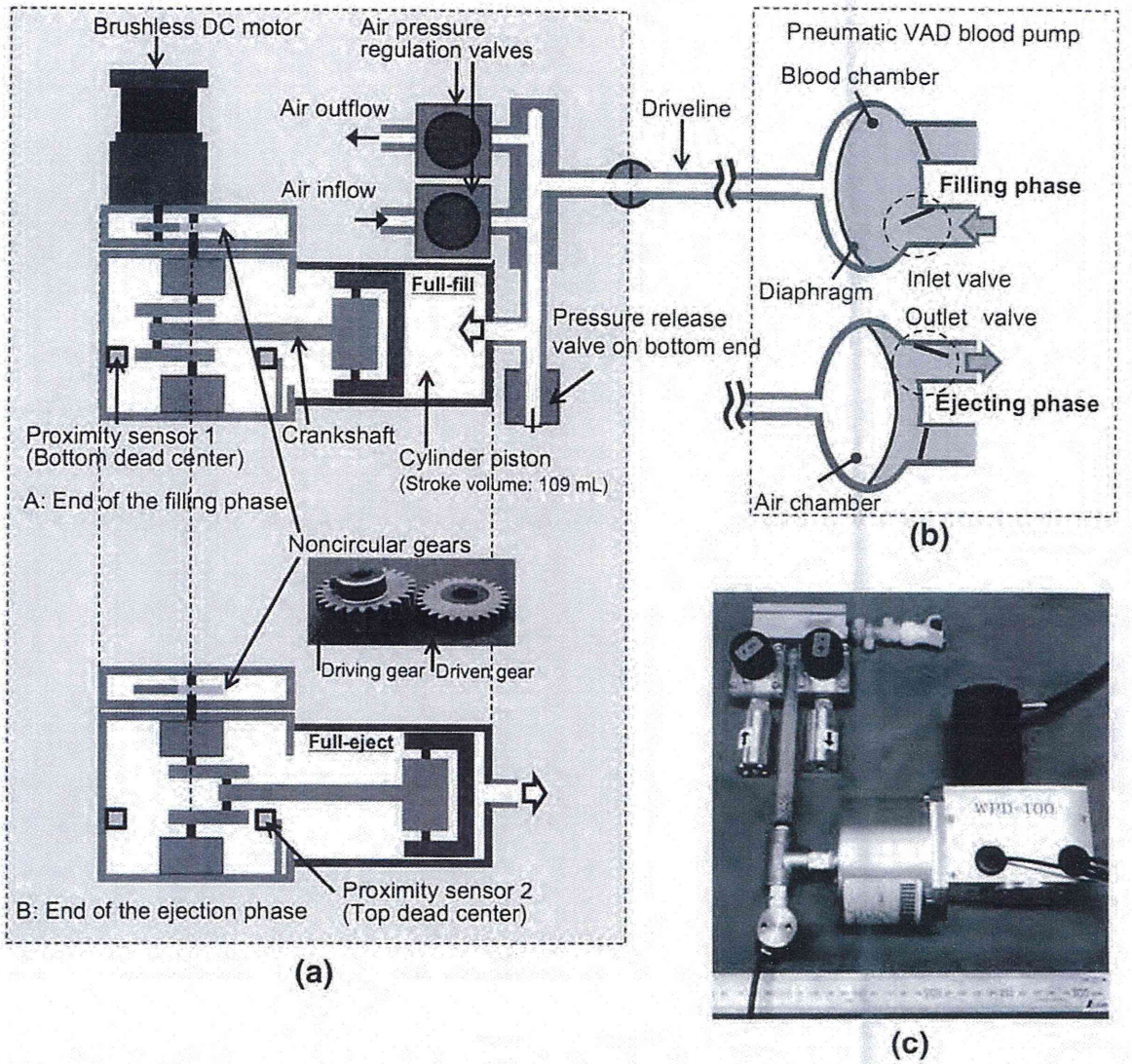

Fig. 1 Overview of the WPD-100 drive unit. **a** WPD-100 mechanism for generating air pressure. **b** Mechanism for generating pulsatile flow on the pneumatic blood pump. **c** Photograph of the core unit, air regulation valves and pressure release valves

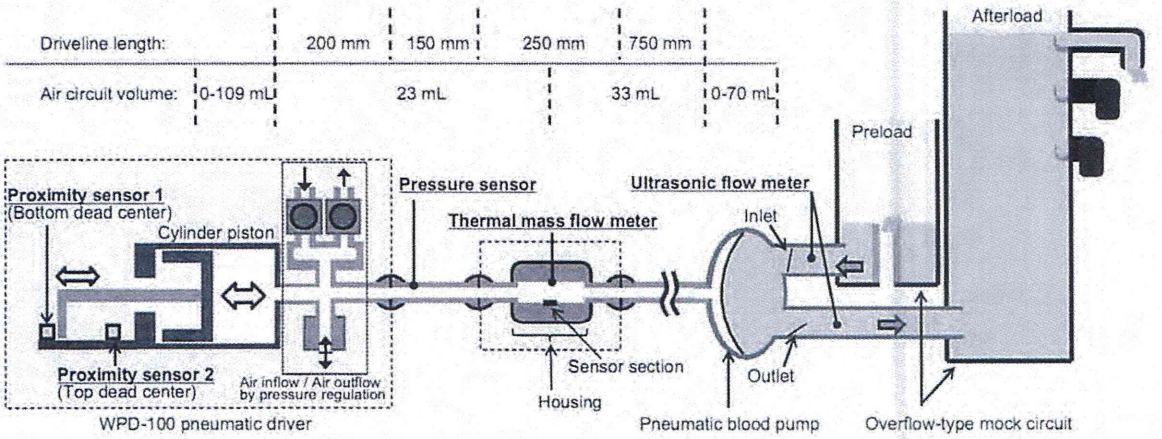

Fig. 2 Schematic diagram of equipment composition and the experimental circuit (air circuit of the pneumatic driver side and mock circuit of the pump output side)

instantaneous value of air temperature in the driveline with high responsiveness.

Test conditions

The preload to the blood pump was kept constant at 10 mmHg using the overflow-type mock circuit, and the afterload was set to 80, 100, and 120 mmHg, respectively. The measurements were conducted with SD ratios of 35, 40, and 45 % using the three types of drive units, and beating rates of 60, 70, 80, 90, and 100 bpm. The pressure of the blood pump was adjusted using the air pressure regulation valves of the drive unit so that almost full filling and full ejection driving was achieved by visual inspection.

Results

Figure 3 shows an example waveform when the blood pump was driven by WPD100-SD40 at 70 bpm, with an afterload of 100 mmHg and a preload of 10 mmHg. The output from the air flow meter demonstrated sufficient response to the ejection and the filling of the VAD. The output of the air flow meter, $Q_{a\ StdF}$, during the filling phase was positive in Fig. 3b because all the air flow passed through the sensor is output as a signal of positive direction, and does not indicate the direction of the air flow. Based on the signal of the proximity sensors of the WPD, we were able to easily divide the waveform into the ejecting phase and the filling phase and to change the waveform direction of the filling phase into the real flow direction as shown in Fig. 3d.

Reflux components generated by the mechanical valve that are not reflected in the air flow rate and flow components for a period during which the inflow and outflow of the pump occur simultaneously were detected (Fig. 3c). Similar trends were also obtained under other driving conditions (Fig. 4a, b). The average of the reflux components shown in Fig. 4a was 0.69 ± 0.077 L/min. Ratios of the flow component shown in Fig. 4b to the pump flow rate were a maximum of 3.9 % (SD 35 %, HR: 100 bpm, afterload: 80 mmHg) and a minimum of 1.3 % (SD 45 %, HR: 60 bpm, afterload: 120 mmHg) under all test conditions.

Figure 3d shows a comparison between the converted air flow rates, $Q_{a\ VF}$, and the blood flow rates, Q_p. During ejection, phase deviation between the air and blood was observed due to compressibility. The deviation is illustrated as the shadowed area between the waveforms of the air flow rate and the blood flow rate in Fig. 3d. The Nipro VAD employs active filling via the negative pressure generated by the vacuum pump in the console, but the deviation was found to be smaller during the filling phase. Similar trends were also obtained under other driving conditions. Except for this deviation, there is sufficient similarity of the outputs from the air flow meter to those from the blood flow meter.

As one example, the significant deviations during the ejecting phase at SD40 are shown in Fig. 4c as the capacity in one cycle under each driving condition. The capacity of the air circuit in the latter part of the air flow meter was approximately 103 mL at the end of the pump ejection phase and approximately 33 mL at the end of the filling phase. As shown in Fig. 4c, the capacity required for compression to raise the pressure of the air of this capacity from 0 to 250 mmHg (approximate value of the maximum driving pressure) was calculated as 18.9 mL from the capacity of the air circuit at the end of the ejection phase and as 6.1 mL from the capacity at the end to the filling phase, using formulae of changes in gas state (2) and (3), where polytropic index, n was set to 1.4.

$$PV^n = \text{const.} \tag{2}$$

$$\frac{V_1}{V_2} = \left(\frac{P_2}{P_1}\right)^{\frac{1}{n}} \tag{3}$$

The average flow rates were obtained by integrating the flow rate waveforms obtained for the ejecting and filling periods. The correlations of the pump outlet flow rate during the ejecting phase and the air flow rates during the ejecting phase are shown in Fig. 5a, and the pump outlet flow rate during the ejecting phase and the air flow rates during the filling phase are shown in Fig. 5b. Good linearity was found in the average air flow rates in the filling directions (in the forward direction, SD45: $R^2 = 0.781$, SD40: $R^2 = 0.704$, SD35: $R^2 = 0.856$; and in the backward direction, SD45: $R^2 = 0.969$, SD40: $R^2 = 0.947$, SD35: $R^2 = 0.971$). However, deviations from the blood flow meter were found both in the ejecting and filling directions. The average flow rate measured by the air flow meter was approximately 90 % lower than that measured by the blood flow meter in the forward direction and approximately 120 % higher in the backward direction.

Discussion

In this study, similarity in the instantaneous waveform was confirmed between the air flow rate in the driveline and the pump flow rate. A significant correlation was particularly recognized between the average blood flow rates and the air flow rates of the filling direction. On the other hand, some limitations of this technique were suggested by the deviation between the air flow and blood flow observed due to compressibility of the air and the error factors that were not reflected in the air flow, as described below.